Fracture toughness parameters to assess crack healing capacity of fiber reinforced concrete under repeated cracking-healing cycles

Estefanía Cuenca, Liberato Ferrara

PII: S0167-8442(19)30688-3
DOI: https://doi.org/10.1016/j.tafmec.2019.102468
Reference: TAFMEC 102468

To appear in: *Theoretical and Applied Fracture Mechanics*

Received Date: 9 November 2019
Revised Date: 21 December 2019
Accepted Date: 27 December 2019

Please cite this article as: E. Cuenca, L. Ferrara, Fracture toughness parameters to assess crack healing capacity of fiber reinforced concrete under repeated cracking-healing cycles, *Theoretical and Applied Fracture Mechanics* (2019), doi: https://doi.org/10.1016/j.tafmec.2019.102468

Fracture toughness parameters to assess crack healing capacity of fiber reinforced concrete under repeated cracking-healing cycles

Estefanía Cuenca

Assistant Professor

Department of Civil and Environmental Engineering

Politecnico di Milano, Milan, Italy

estefania.cuenca@polimi.it

Liberato Ferrara

Associate Professor

Department of Civil and Environmental Engineering

Politecnico di Milano, Milan, Italy

liberato.ferrara@polimi.it

ABSTRACT

This paper is the continuation of a research focused on the assessment of the crack-sealing capacity of Steel Fiber Reinforced Concrete (SFRC) with crystalline admixtures subjected to repeated cracking-healing cycles. In the first study, the work was focused on the quantitative evaluation of the crack-sealing performance by means of image analysis. To this purpose, crack sealing effectiveness was evaluated as a function of the presence of crystalline admixtures, maximum crack opening, duration of the healing period, exposure conditions (immersion in water, exposure to open-air exposure or wet/dry cycles), fiber orientation and number of cracking and healing cycles. The outcomes of the self-sealing phenomenon were analyzed defining a crack-sealing index calculated from images taken by means of a digital microscope both at the beginning and at the end of each healing exposure period. In this paper, it has been tried to move a step further, correlating the Sealing Index (crack closure in %) with parameters obtained from fracture toughness tests on specimens subjected to repeated cracking-healing cycles, with the aim of quantifying the retention and/or recovery of mechanical properties along the testing path. This is meant to simulate a real structural service scenario, in which a healed crack may reopen and be allowed enough time to re-heal, this repetition of events being likely to occur several times during the structure service life. To this purpose, equivalent tensile stresses (obtained from absorbed energy per unit fracture surface) were determined from nominal tensile stress vs. crack opening displacement curves obtained from a dedicated testing methodology, namely the Double Edge Wedge Splitting (DEWS) tests, and their evolution along the cracking and healing cycles was assessed. Results showed that, an increase of the Sealing Index, *i.e.* a more effective sealing of the cracks, also results into a slight increase of SFRC toughness performances as a consequence of both the through-crack matrix continuity reconstitution as well as of a likely improved bond between fibers and matrix. The method proposed in the paper can be further employed to build up a data-base in order to establish, through suitable meta-analysis procedure, sound correlation between parameters representative of crack self-sealing and material performance recovery (self-healing).

Keywords: Self-healing; Crystalline admixtures; steel fibers; toughness

Notations:

σ_{eq}=equivalent tensile stress [MPa];

$\sigma_{eq,cycle}$ =equivalent tensile stress in a cycle [MPa];

$\sigma_{eq,total}$ =equivalent tensile stress of all cycles [MPa];

$F_{sp,\ average}$ = Resulting tensile force of the ligament [N];

σ_N= nominal tensile stress [MPa];

t = specimen thickness [mm];

h_{lig} = ligament depth [mm];

w = crack width;

W_F = absorbed energy per unit fracture surface [MPa·mm]

1. INTRODUCTION

The implementation of the sustainability concept into the field of cement-based construction materials [1] has led to relentless and successful efforts in the concept and application of materials whose signature enhanced performance. This has not to be merely limited to higher strength but, even more importantly, has also to be characterized by a somewhat intrinsic ability of providing, also through a better interaction with conventional reinforcement, a better control of deformation and cracking under the intended structural service scenario [2]. While the former could result into the use of lower material quantities for building structural elements and components equally performing in the ultimate limit state, the second could actually lead to a more efficient use of the material appropriately resulting into longer duration of the engineering feat. As a matter of fact, a more efficient control of the cracking contributes to delay the penetration of aggressive agents, hence delaying also the aging and degradation of the material and structural performance in the overall framework of a better response to mechanical and environmental actions [2].

Fiber Reinforced Concrete (FRC) and Fiber Reinforced Cementitious Composites (FRCCs) do clearly personify the aforementioned concept, also through the availability of widely validated design rules in several national and international standards and codes, and are nowadays prominent actors in the field of civil and building engineering.

In the last decade or so, the sustainability signature of cement-based construction materials has been further enriched with the worth of autogenous and engineered healability of the material and structural performance [3]. Fibre Reinforced Concrete and Cementitious Composites do also embody this further value through the synergic effect on the one hand of signature features of the material composition (including higher content of binders, optimized w/c ratios) which can enhance the autogenous delayed-hydration related self-healing capacity, and, on the other hand, right because of the inborn enhanced crack control capacity [4]. A crack pattern characterized by finer and more regularly distributed cracks is more easily healable.

The studies of the self-healing capacity of concrete and cement based materials have nowadays reached a good maturity at the material level [5, 6], ready to be scaled-up to the aforementioned concept of the *healability* of the "in-structure" material performance, also through the incorporation of the same concepts into suitable design approaches, e.g. through the definition of a scenario-dependent healable crack concept [7].

In the case of fiber reinforced concrete and cementitious composites, the healability of the in-structure material performance has to be evaluated as the synergy between the closure of the crack and the ability of the material to maintain its target level of post-cracking residual tensile strength as the outcome of through-crack continuity reconstruction [8-13].

Such a multifold concept becomes of the utmost importance, mainly in the case of repeated cracking and healing cycles, which are likely to characterize the majority of the structural service scenarios for several engineering applications. In this respect the authors have proposed and validated a methodology aimed at assessing the crack sealing capacity of fiber-reinforced concrete upon repeated cracking and healing cycles [14]. The proposed methodology employs the Double Edge Wedge Splitting test [15], which has been demonstrated able to yield straightforward. *i.e.* without the need of a back analysis, the tensile stress vs. crack opening relationship of the fiber-reinforced composite. In view of this, the performed experimental investigation has made available the complete tensile stress vs. crack-opening curves of the investigated materials upon the performed successively repeated cycles of cracking and healing, thus providing valuable information on the capacity of the material to retain, under the simulated scenario, its fracture toughness performance [16], to which its long term "durability related" design parameters are strictly correlated.

In this paper, the aforementioned properties will be thoroughly analyzed with a tailored and appropriately calibrated methodology and correlated with the already validated database on the crack sealing capacity [14], in an attempt to pave the way to incorporate, through suitable performance based approaches, the outcomes of self-healing into structural design methodologies. This is also meant to foster the implementation and market penetration of the broad category of self-healing advanced fiber reinforced cement-based materials.

2. EXPERIMENTAL PROGRAM AND TEST SETUP

Two concrete mixes were analyzed. A reference steel fiber reinforced concrete (SFRC) and a second mix containing a crystalline admixture (SFRC+CA) in order to study its effectiveness as stimulator of the healing capacity. Mix composition for both concretes is shown in Table 1. The employed crystalline admixture is a commercial product which has been already extensively studied by the authors with reference to both its

chemical characteristics [17] as well as to its use as healing stimulator in a wide variety of cement-based materials as well as to a broad range of exposure scenarios.

Compressive strength (EN 12390-3) and flexural toughness (EN 14651) tests were performed to properly characterize both concretes. From flexural toughness tests, the limit of proportionality (f_{ctl}) and the residual flexural tensile strength ($f_{R,j}$) were determined corresponding to the crack mouth opening displacements (CMOD) equal to 0.5, 1.5, 2.5 and 3.5 mm (j=1, 2, 3, 4 respectively). Table 2 shows the mechanical properties of both mixes, giving the average values of compressive strength (f_c) and of all the residual flexural strengths, together with standard deviations in brackets. All the mechanical values were obtained as the average of at least three (if not otherwise specified) specimens 28 days after casting the specimens.

Table 1. Concrete mix design (kg/m^3)

Constituent	**SFRC**	**SFRC+CA**
Cement type II 42.5	360	360
Sand (0-4mm)	814	811
Coarse aggregate (4-16mm)	1077	1077
Water	180	180
Superplasticizer	3.5	3.5
Steel fibers (l_f= 60 mm; d_f= 0.92 mm)	40	40
Crystalline admixture	0	2.9

Table 2. Concrete mechanical properties at 28 days (standard deviation in brackets)

	SFRC	**SFRC+CA**
Compressive strength. f_c [MPa]	46.6 (3.84)	41.2 (3.62)
Residual flexural strength:		
f_{R1} [MPa]	7.60 (0.03)	6.08 (0.80)
f_{R2} [MPa]	8.38 (0.52)	9.29 (0.75)
f_{R3} [MPa]	8.46 (0.06)	9.08 (0.32)
f_{R4} [MPa]	8.14 (0.03)	7.78 (0.94)

To analyze the effectiveness of this crystalline admixture as a healing promoter, a comprehensive campaign was carried out. The variables involved are shown in Table 3. The complete experimental program is comprehensively explained in Cuenca et al. [14] and will be briefly summarized hereafter.

Table 3. Main variables and studied levels

Variable	**Levels**
First healing exposure period	1 month, 6 months
Exposure healing conditions	Water, air exposure, wet/dry cycles
Presence of crystalline admixtures	Yes/No
Fiber alignment with respect to the crack	Favorable / Unfavorable

Pre/re-cracking tests (Figure 1) were carried out through Double Edge Wedge Splitting (DEWS) tests developed by di Prisco et al. [15] performed up to a crack opening of 0.25mm (Figure 1). 150 mm square-side and 50 mm thick specimens were employed, with a groove and a notch cut to single-out a 110 mm long ligament cross section. As explained in detail by Cuenca et al. [14] such specimens were cut out from prismatic beams specimens (150x150x600 mm) in such a way to obtain different orientations of the fibers with respect to the ligament cross sections. After first cracking, which was performed 4 months after casting [6], the specimens underwent an initial healing period for either 1 or 6 months (itineraries FT-1 and FT-6), being exposed to either one of the following conditions: immersion in tap water, air exposure and wet/dry cycles (each cycle consisted of immersion in tap water for 3 days, followed by exposure to air for 2 days). After the first healing period, specimens were subjected to cracking-healing cycles up to one year according to the scheme shown in Figure 2, respectively. For example, specimens from FT-6 followed this procedure: pre-cracking up to 0.25mm, self-healing exposure for 6 months (for each three exposure conditions), re-cracking up to 0.25mm, healing exposure for 1 month, re-cracking up to 0.25mm, healing exposure for 2 months, re-cracking up to 0.25mm, healing exposure for 1 month, re-cracking up to 0.25mm and healing exposure for 2 months. In this work, the study has been focused in the itineraries FT-1 and FT-6.

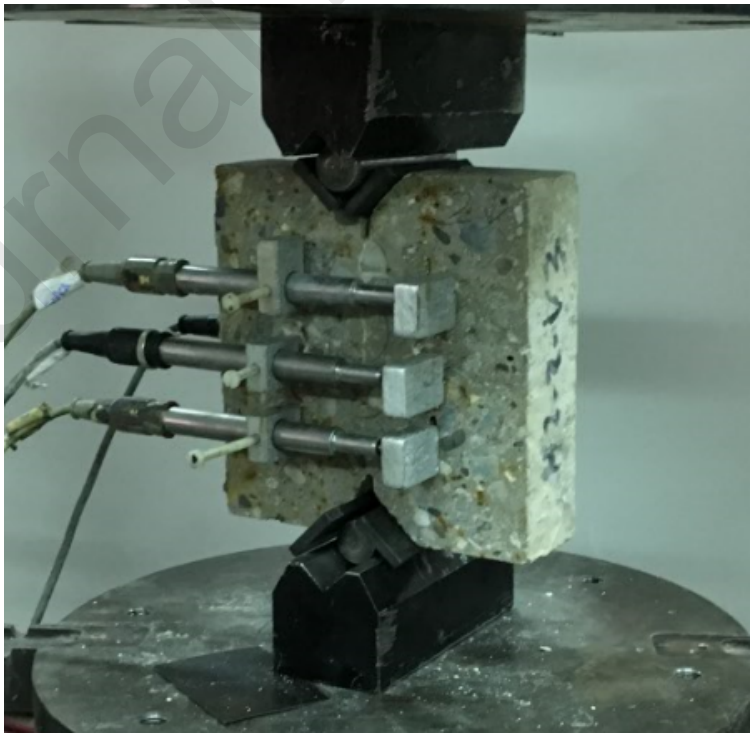

Figure 1. Cracking test setup

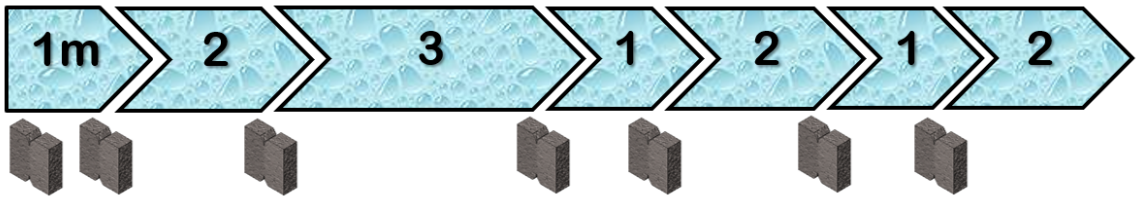

(a)

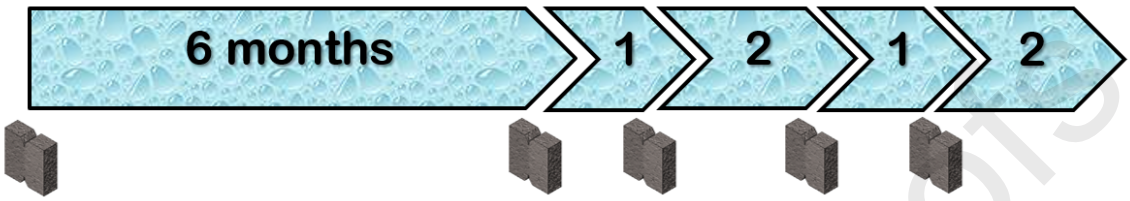

(b)

Figure 2. Scheme of cracking-healing cycles: (a) FT1: treatment schedule characterized by an initial healing exposure of 1 month; (b) FT6: treatment schedule characterized by an initial healing exposure of 6 months

Before and after each healing period, the entire crack was photographed by means of a digital microscope and then, with an image-editing software, the area of the crack before and after healing was quantified by means of a binary image (Figure 3) to determine the crack closure (%). As already underlined, the detailed procedure is explained in Cuenca et al. [14].

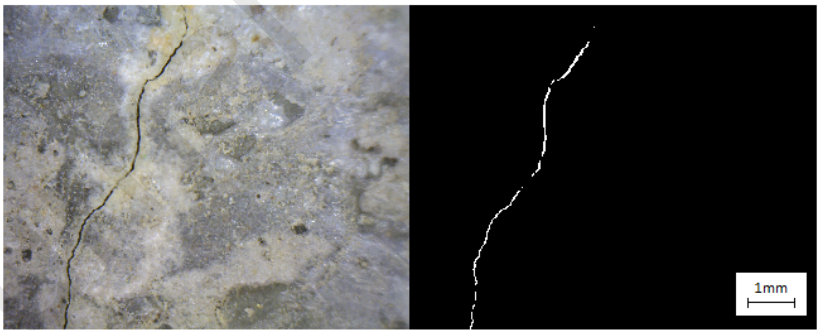

(a)

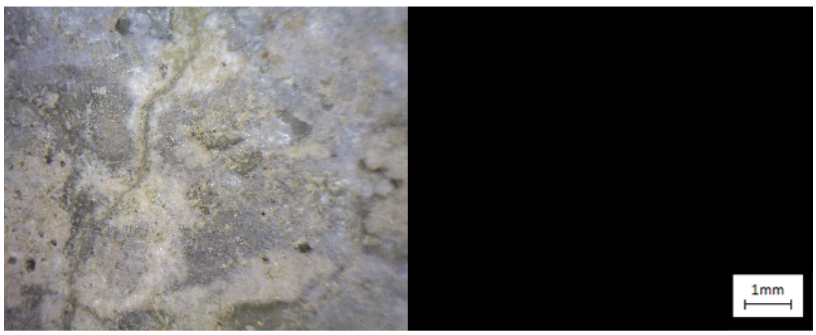

(b)

Figure 3. Original picture and binary image of a crack: (a) after cracking; (b) after healing treatment

3.DATA ANALYSIS METHOD

This study is intended to analyze fracture toughness parameters to assess crack healing capacity. To this purpose reference has been made, for each and all the specimens, to the nominal tensile stress vs. crack opening displacement obtained from the DEWS tests (Figure 4) after repeated cracking-healing cycles for the two test-paths investigated (first healing period of 1 or 6 months) and fiber orientation (favorable: fibers mainly oriented perpendicularly to the crack; unfavorable: mainly parallel to the crack). The nominal tensile stress determined using Eq.1:

$$\sigma_N[MPa] = \frac{\mathrm{F_{sp}[N]}}{cross\ sectional\ area} = \frac{\mathrm{F_{sp}[N]}}{t \cdot h_{lig}} \qquad \text{(Eq.1)}$$

where t is the specimen thickness (50 mm) and h_{lig} the depth of the ligament cross section between the two notches.

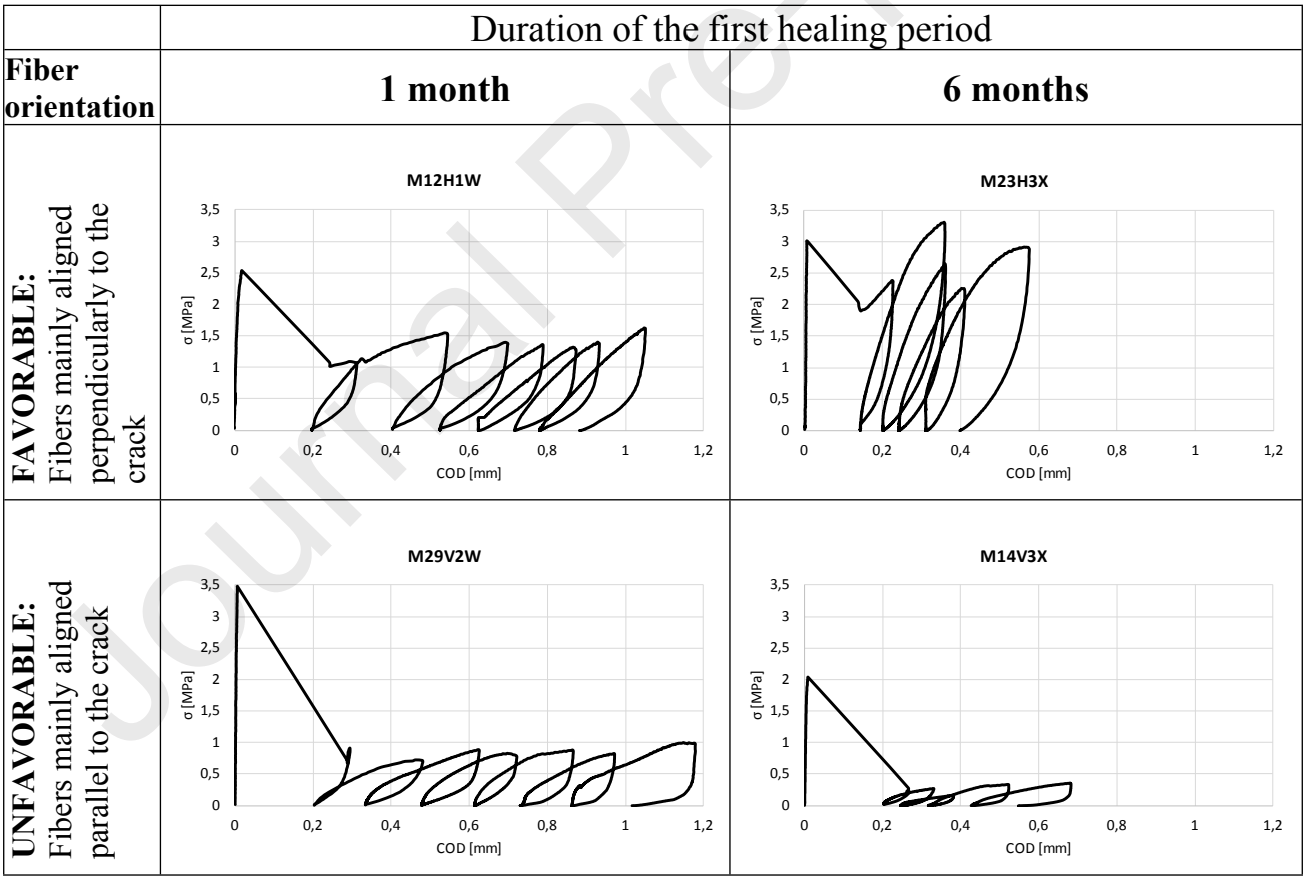

Figure 4. Examples of σ_N - COD curves (nominal tensile stress versus crack opening displacement) as a function of main fiber alignment and duration of the first healing period. The plotted COD is the average of the three measurements taken on either face of the specimen as shown in Figure 1.

Where F_{sp} is the splitting load orthogonal to the ligament cross section of the specimen, calculated from the applied vertical load through free body equilibrium and accounting for the friction between the loading application devices (see Figure 5, based on [15])

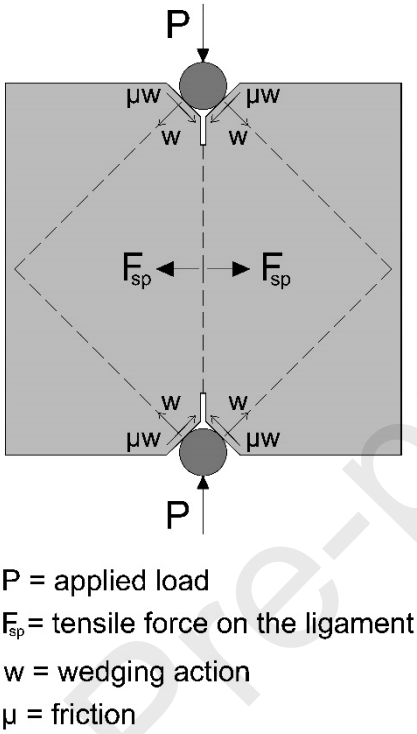

Figure 5. Force scheme in a Double Edge Wedge Splitting (DEWS) test specimen (based on [15])

In Figure 4, it can be observed, as expectable, a higher residual tensile load-bearing capacity for specimens have fibers mainly oriented perpendicularly to the crack (favorable orientation) compared to those with fibers mainly oriented parallel to the crack (unfavorable orientation). This aspect was observed not only for the first loading cycle but also for the other post-healing cracking cycles up to one year. It was furthermore generally observed that the transverse splitting tensile stress was higher for all the cracking cycles when the duration of the first healing period was 6 months as compared to 1 month. It can be reasonably hypothesized that a longer first healing period allowed a more complete development of inside the crack healing products, which are also likely to increase the bond between fibers and concrete, thus increasing the transverse splitting tensile force.

Fracture toughness parameters were determined from the DEWS test results since, due to their purposely conceived geometry, a pure mode I fracture takes place along the ligament [9]. Toughness of the FRC by DEWS

tests can be determined by the area under the nominal tensile stress vs. crack opening displacement curve (σ_N-COD), this is "absorbed energy per unit fracture surface" (W_F).

As a matter of fact, in order to analyze the fracture toughness to assess healing capacity under repeated cracking-cycles several parameters have been obtained from the cracking-healing curves. Figure 6 shows an example of nominal tensile stress (σ_N) versus crack width displacement curve (COD) indicating the methodology to obtain the fracture toughness parameters.

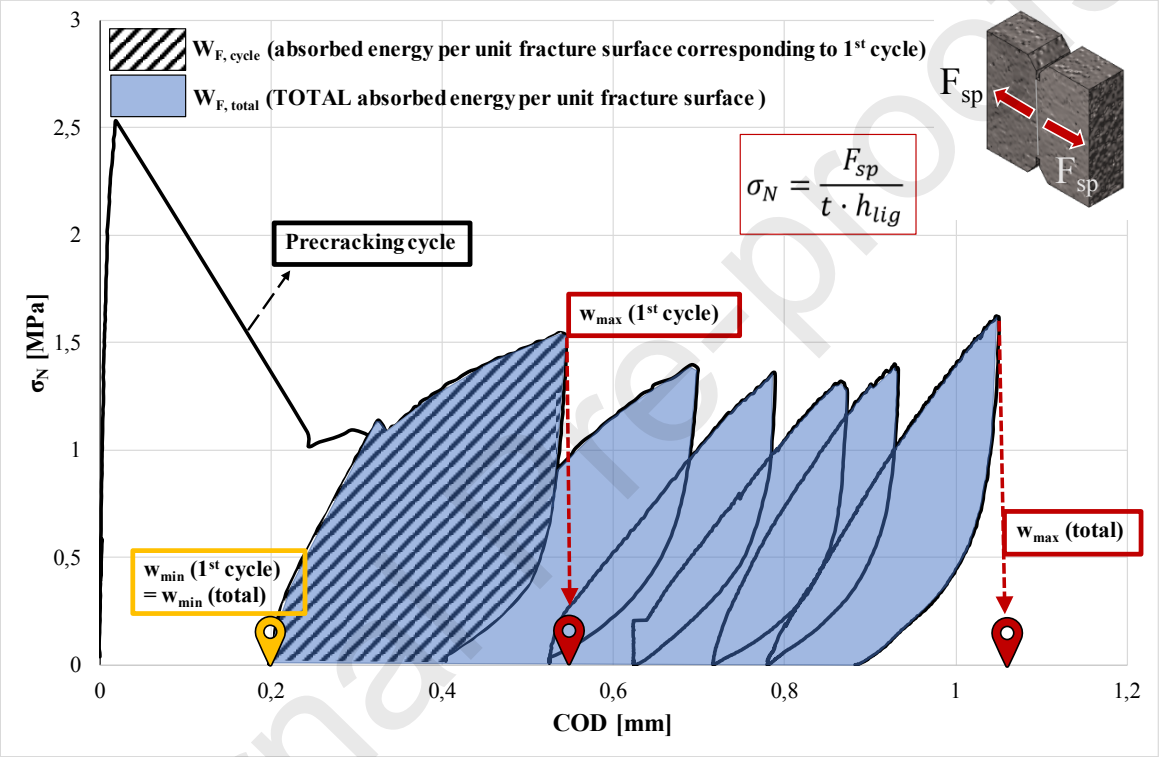

Figure 6. Example of nominal tensile stress (σ_N) versus crack opening displacement (COD). Methodology definition to obtain the absorbed energy per unit fracture surface (W_F) . The plotted COD is the average of the three measurements taken on either face of the specimen as shown in Figure 1.

As shown in Figure 6, it was determined the work of fracture each cycle ($W_{F,cycle}$) and also for all cycles ($W_{F,total}$). From W_F and the crack width variation (Δw) an equivalent tensile stress (σ_{eq}) can be calculated by means of Eq.2:

$$\sigma_{eq}[MPa] = \frac{W_F\ [\text{MPa·mm}]}{\Delta w\ [\text{mm}]} = \frac{W_F\ [\text{MPa·mm}]}{(w_{max} - w_{min})[\text{mm}]} \qquad \text{(Eq.2)}$$

4.ANALYSIS OF RESULTS

The aim of this work is to analyze the above mentioned mechanical and toughness parameters and relate them with the Sealing Index [%] obtained by means of the crack closure after each healing period. The detailed procedure to obtain the latter is explained in [14]. For the sake of this paper it is worth remarking that, once the crack was completely imaged by means of micrographs and the image converted into binary format, the crack area could be calculated for each step of the experimental program detailed above.

The Sealing Index is henceforth calculated as follows, with reference to healing cycle j which follows cracking cycle j-1:

$$\text{Sealing Index (\%)} = \frac{(Crack\ area)_{cracking(j-1)} - (Crack\ area)_{healing(j)}}{(Crack\ area)_{cracking(j-1)}} \cdot 100$$

(Eq. 3)

For each specimen and for each single cycle the Sealing Index [%] was determined. Table 4 and Table 5 summarize the main parameters used in the analysis (W_F, $\Delta w = w_{max}$-w_{min}, $\sigma_{eq,cycle}$, Sealing Index [%], relative equivalent tensile stress = $\sigma_{eq,cycle}$ /$\sigma_{eq,total}$) and the duration of the healing, age, crack size for each specimen identified by a specimen identity (Specimen ID) that follows the following structure: type of mix (M1, without crystalline admixtures; M2, with crystalline admixtures), DEWS number, fiber orientation (H1, H2, H3, V1, V2, V3 as indicated in [6]), exposure condition (W: water immersion, X: wet/dry cycles, A: air exposure), number of cracking-healing cycle. For example: M14H2X_5 is an identification regarding to the 5th crack-healing cycle ("_5") of a specimen made with concrete without crystalline admixtures (M1), specimen number 4, fiber orientation H2, subjected to wet/dry cycles.

Table 4. Main results regarding specimens healed for 1 month (continued on next page) – 1/3

Specimen ID	Age (months)	Crack size	W_F [MPa·mm]	w_{max}-w_{min} [mm]	$\sigma_{eq.cycle}$ [MPa]	Sealing Index [%]	Relative equivalent tensile stress = $\sigma_{eq,cycle}$ /$\sigma_{eq,total}$
M11H1W_1	1	small	0.214	0.262	0.820	18.4	0.613
M12H1W_1	1	small	0.305	0.348	0.878	70.2	0.863
M12H2W_1	1	small	0.315	0.275	1.149	77.1	0.702
M12H1W_2	3	small	0.184	0.291	0.633	32.9	0.622
M12H2W_2	3	small	0.194	0.224	0.865	25.9	0.529
M12H1W_4	9	small	0.136	0.233	0.583	50.3	0.572
M12H2W_4	9	small	0.352	0.271	1.300	28.6	0.795
M11H1W_5	10	small	0.392	0.311	1.262	79.6	0.944
M12H1W_5	10	small	0.116	0.208	0.557	91.7	0.547
M12H2W_5	10	small	0.285	0.242	1.179	94.0	0.721
M11H1W_6	12	small	0.244	0.238	1.024	58.3	0.766
M12H1W_6	12	small	0.162	0.266	0.610	77.9	0.599
M12H2W_6	12	small	0.367	0.287	1.278	93.1	0.781
M11H1W_2	3	medium	0.090	0.128	0.704	43.8	0.526
M13H1X_1	1	small	0.283	0.268	1.053	11.2	0.642
M19H1X_1	1	small	0.347	0.305	1.137	60.6	0.699
M14H2X_1	1	small	0.254	0.291	0.871	57.5	0.763
M19V2X_1	1	small	0.131	0.116	1.130	43.5	0.524
M13H1X_2	3	small	0.043	0.056	0.771	40.5	0.470
M19H1X_2	3	small	0.189	0.203	0.929	20.2	0.571
M19V2X_2	3	small	0.175	0.160	1.097	52.8	0.509
M19H1X_4	9	small	0.159	0.185	0.863	46.3	0.530
M14H2X_4	9	small	0.218	0.263	0.829	30.0	0.726
M19V2X_4	9	small	0.158	0.162	0.974	1.1	0.452
M19H1X_5	10	small	0.263	0.231	1.138	54.2	0.699
M19V2X_5	10	small	0.376	0.247	1.522	13.5	0.706
M19H1X_6	12	small	0.349	0.274	1.276	92.7	0.784
M14V2X_1	1	medium	0.616	2.056	0.300	36.1	1.054
M13H1X_4	9	medium	0.307	0.260	1.184	7.7	0.722
M13H1X_5	10	medium	0.177	0.206	0.860	30.3	0.525
M14H2X_5	10	medium	0.219	0.261	0.838	77.5	0.734
M13H1X_6	12	medium	0.472	0.327	1.446	33.5	0.882
M14H2X_6	12	medium	0.261	0.279	0.939	66.9	0.822
M19V2X_6	12	medium	0.648	0.350	1.850	38.9	0.859
M14V2X_2	3	large	0.056	0.291	0.194	22.5	0.682

Table 4. Main results regarding specimens healed for 1 month (continued on next page) – 2/3

Specimen ID	Age (months)	Crack size	W_F [MPa·mm]	w_{max}-w_{min} [mm]	$\sigma_{eq.cycle}$ [MPa]	Sealing Index [%]	Relative equivalent tensile stress = $\sigma_{eq,cycle}$ /$\sigma_{eq,total}$
M14V2X_4	9	large	0.014	0.147	0.097	7.4	0.341
M14V2X_5	10	large	0.016	0.200	0.081	4.8	0.286
M15H1A_1	1	small	0.424	0.323	1.311	48.6	0.749
M15H1A_2	3	small	0.206	0.226	0.909	24.6	0.519
M19V3A_1	1	medium	0.037	0.200	0.185	30.1	0.859
M16H2A_2	3	large	0.018	0.165	0.110	0.0	0.369
M15H1A_4	9	large	0.299	0.233	1.282	13.2	0.732
M16H2A_4	9	large	0.047	0.221	0.214	6.3	0.717
M19V3A_4	9	large	0.031	0.249	0.125	0.0	0.583
M15H1A_5	10	large	0.245	0.229	1.069	25.9	0.610
M16H2A_5	10	large	0.023	0.234	0.098	9.7	0.330
M19V3A_5	10	large	0.024	0.242	0.100	0.0	0.466
M16H2A_6	12	large	0.101	0.271	0.372	11.6	1.248
M19V3A_6	12	large	0.025	0.229	0.110	28.1	0.513
M22H2W_1	1	small	0.015	0.076	0.200	78.3	0.339
M22H2W_6	12	small	0.088	0.233	0.376	100.0	0.635
M29V2W_1	1	medium	0.089	0.273	0.326	91.7	0.544
M21H1W_4	9	medium	0.107	0.286	0.374	0.0	0.577
M29V2W_4	9	medium	0.121	0.240	0.506	70.3	0.843
M21H1W_5	10	medium	0.172	0.257	0.670	52.4	1.034
M29V2W_5	10	medium	0.100	0.230	0.434	75.8	0.722
M21H1W_6	12	medium	0.082	0.261	0.312	28.9	0.482
M29V2W_6	12	medium	0.178	0.314	0.568	65.2	0.946
M21H1W_1	1	large	0.055	0.231	0.237	33.8	0.366
M24V2X_1	1	small	0.106	0.247	0.428	48.0	0.539
M23H1X_1	1	medium	0.759	0.540	1.404	35.4	0.899
M24H2X_1	1	medium	0.083	0.239	0.346	8.0	0.670
M24V2X_2	3	medium	0.104	0.205	0.506	25.2	0.637
M24V2X_4	9	medium	0.168	0.209	0.805	27.6	1.013
M24V2X_5	10	medium	0.128	0.224	0.571	43.2	0.720
M24V2X_6	12	medium	0.145	0.247	0.589	29.9	0.742
M23H1X_2	3	large	0.246	0.316	0.781	0.0	0.499
M23H1X_4	9	large	0.275	0.278	0.991	0.0	0.634
M24H2X_4	9	large	0.049	0.199	0.247	23.7	0.480
M23H1X_5	10	large	0.180	0.255	0.704	17.8	0.451
M24H2X_5	10	large	0.090	0.259	0.348	29.8	0.675

Table 4. Main results regarding specimens healed for 1 month (continued) – 3/3

Specimen ID	Age (months)	Crack size	W_F [MPa·mm]	w_{max}-w_{min} [mm]	$\sigma_{eq.cycle}$ [MPa]	Sealing Index [%]	Relative equivalent tensile stress = $\sigma_{eq,cycle}$ /$\sigma_{eq,total}$
M23H1X_6	12	large	0.271	0.308	0.881	12.3	0.564
M24H2X_6	12	large	0.086	0.262	0.329	22.4	0.639
M25H1A_1	1	small	0.108	0.245	0.439	31.3	0.734
M26V1A_1	1	small	0.076	0.286	0.265	23.6	0.549
M25H1A_2	3	small	0.079	0.333	0.237	28.8	0.397
M25H1A_4	9	medium	0.059	0.184	0.319	0.0	0.533
M26H2A_1	1	large	0.100	0.275	0.364	27.7	0.494
M26H2A_4	9	large	0.138	0.268	0.517	0.0	0.701
M26V1A_4	9	large	0.104	0.251	0.415	3.6	0.860
M25H1A_5	10	large	0.066	0.159	0.413	0.0	0.690
M26H2A_5	10	large	0.144	0.257	0.560	17.5	0.759
M26V1A_5	10	large	0.047	0.172	0.270	1.2	0.559
M25H1A_6	12	large	0.036	0.109	0.330	15.9	0.551
M26H2A_6	12	large	0.147	0.252	0.583	20.4	0.790
M26V1A_6	12	large	0.095	0.268	0.355	12.4	0.735
M25H1A_7	12	large	0.103	0.218	0.473	24.1	0.791

Table 5. Main results regarding specimens healed for 6 months (continued on next page) – 1/3

Specimen ID	Age (months)	Crack size	W_F [MPa·mm]	w_{max}-w_{min} [mm]	$\sigma_{eq,cycle}$ [MPa]	Sealing Index [%]	Relative equivalent tensile stress = $\sigma_{eq,cycle}$ /$\sigma_{eq,total}$
M18H3W_1	7	small	0.185	0.150	1.240	100.0	0.766
M16H1W_2	9	small	0.120	0.202	0.596	58.1	0.526
M16V3W_2	9	small	0.263	0.311	0.846	100.0	1.001
M18H3W_2	9	small	0.090	0.129	0.703	67.6	0.434
M16H1W_3	10	small	0.166	0.248	0.671	45.9	0.593
M16V3W_3	10	small	0.110	0.223	0.493	100.0	0.584
M18H3W_3	10	small	0.355	0.250	1.424	100.0	0.879
M15H2W_4	12	small	0.141	0.276	0.510	100.0	0.851
M16H1W_4	12	small	0.198	0.250	0.793	86.7	0.701
M15H2W_1	7	medium	0.092	0.152	0.606	100.0	1.012
M16V3W_1	7	medium	0.041	0.123	0.333	100.0	0.394
M18H3W_4	12	medium	0.186	0.233	0.796	99.0	0.492
M16H1W_1	7	large	0.250	0.263	0.951	92.6	0.840
M13H3X_1	7	small	0.328	0.252	1.302	80.5	0.787
M14H1X_1	7	small	0.145	0.157	0.925	99.2	0.823
M13H3X_2	9	small	0.086	0.146	0.586	25.7	0.354
M14H1X_2	9	small	0.083	0.142	0.584	88.3	0.519
M14V3X_2	9	small	0.007	0.125	0.053	23.2	0.274
M18H2X_2	9	small	0.245	0.265	0.923	57.8	0.921
M14H1X_3	10	small	0.101	0.155	0.649	75.9	0.578
M14V3X_3	10	small	0.034	0.197	0.172	100.0	0.889
M14H1X_4	12	small	0.183	0.226	0.812	54.6	0.723
M14V3X_4	12	small	0.042	0.244	0.172	97.2	0.886
M14V3X_1	7	medium	0.015	0.118	0.130	92.3	0.672
M18H2X_1	7	medium	0.123	0.197	0.625	100.0	0.624
M13H3X_3	10	medium	0.218	0.197	1.107	36.1	0.669
M18H2X_3	10	medium	0.165	0.255	0.649	76.8	0.648
M13H3X_4	12	medium	0.267	0.231	1.156	47.9	0.699
M18H2X_4	12	medium	0.161	0.254	0.632	61.8	0.631
M11H2A_1	7	medium	0.132	0.258	0.512	13.4	0.783
M12V3A_1	7	medium	0.017	0.079	0.214	17.9	0.389
M12V3A_2	9	medium	0.033	0.131	0.253	0.0	0.460
M18H1A_1	7	large	0.214	0.259	0.825	5.8	0.706
M11H2A_2	9	large	0.110	0.261	0.421	15.5	0.642
M18H1A_2	9	large	0.053	0.101	0.526	4.9	0.450
M11H2A_3	10	large	0.059	0.201	0.292	0.0	0.447
M12V3A_3	10	large	0.104	0.213	0.489	12.4	0.890
M18H1A_3	10	large	0.149	0.220	0.679	10.5	0.581
M11H2A_4	12	large	0.124	0.283	0.438	0.0	0.669

Table 5. Main results regarding specimens healed for 6 months (continued on next page) – 2/3

Specimen ID	Age (months)	Crack size	W_F [MPa·mm]	wmax-wmin [mm]	σeq.cycle [MPa]	Sealing Index [%]	Relative equivalent tensile stress = $\sigma_{eq,cycle}/\sigma_{eq,total}$
M12V3A_4	12	large	0.111	0.257	0.434	7.0	0.790
M18H1A_4	12	large	0.275	0.271	1.018	19.9	0.871
M28H3W_2	9	small	0.277	0.217	1.273	100.0	0.998
M25H2W_3	10	small	0.044	0.359	0.123	100.0	0.677
M28H3W_3	10	small	0.135	0.199	0.681	100.0	0.534
M28H3W_4	12	small	0.192	0.211	0.909	100.0	0.712
M25H2W_1	7	medium	0.037	0.204	0.182	99.1	1.006
M26V3W_1	7	medium	0.041	0.113	0.363	100.0	0.401
M28H3W_1	7	medium	0.086	0.139	0.623	100.0	0.488
M26V3W_2	9	medium	0.063	0.121	0.523	91.7	0.578
M26V3W_3	10	medium	0.252	0.252	1.001	95.6	1.106
M26V3W_4	12	large	0.202	0.252	0.802	60.8	0.885
M28H2X_4	12	small	0.024	0.260	0.092	23.5	0.712
M23H3X_1	7	medium	0.359	0.211	1.699	95.6	0.790
M24V3X_1	7	medium	0.028	0.243	0.114	44.6	0.699
M23H3X_2	9	medium	0.209	0.148	1.415	60.8	0.658
M24V3X_2	9	medium	0.025	0.224	0.113	26.5	0.697
M28H2X_2	9	medium	0.014	0.195	0.070	22.5	0.543
M23H3X_3	10	medium	0.203	0.155	1.314	52.6	0.611
M24V3X_3	10	medium	0.032	0.268	0.118	20.1	0.726
M28H2X_3	10	medium	0.021	0.264	0.080	48.5	0.619
M23H3X_4	12	medium	0.459	0.252	1.821	39.7	0.847
M24H1X_1	7	large	0.084	0.102	0.829	22.7	0.460
M28H2X_1	7	large	0.028	0.257	0.109	60.7	0.843
M24H1X_2	9	large	0.224	0.207	1.082	37.4	0.600
M24H1X_3	10	large	0.399	0.248	1.612	43.0	0.894
M24H1X_4	12	large	0.387	0.249	1.553	4.8	0.861
M24V3X_4	12	large	0.069	0.414	0.166	38.6	1.020
M22H1A_1	7	medium	0.408	0.285	1.432	28.3	0.947
M22V1A_1	7	medium	0.075	0.179	0.421	29.2	0.600
M28H1A_1	7	medium	0.035	0.110	0.315	12.8	0.510
M22V1A_2	9	medium	0.149	0.213	0.699	0.0	0.997
M28H1A_2	9	medium	0.125	0.185	0.677	21.5	1.096
M22H1A_3	10	medium	0.120	0.185	0.651	1.7	0.431
M22V1A_3	10	medium	0.120	0.198	0.606	4.8	0.864
M22H1A_2	9	large	0.046	0.102	0.454	24.7	0.300
M28H1A_3	10	large	0.039	0.139	0.284	0.0	0.459

Table 5. Main results regarding specimens healed for 6 months (continued) – 3/3

Specimen ID	Age (months)	Crack size	W_F [MPa·mm]	wmax-wmin [mm]	σeq.cycle [MPa]	Sealing Index [%]	Relative equivalent tensile stress = $\sigma_{eq,cycle}$ /$\sigma_{eq,total}$
M22H1A_4	12	large	0.260	0.240	1.082	4.9	0.716
M22V1A_4	12	large	0.063	0.189	0.333	0.0	0.475
M28H1A_4	12	large	0.099	0.253	0.390	11.8	0.631

4.1 Cycle-equivalent tensile stress vs. Sealing Index

Figure 7 shows the equivalent tensile stress for each cycle as a function of Sealing Index for both FT-1 and FT-6. In FT-1 specimens it can be observed that the equivalent tensile stress seems to slightly increase for higher Sealing Index values, while in FT-6 the influence was milder. Moreover, for large cracks in specimens subjected to the same exposure condition, those with crystalline admixtures reached higher equivalent tensile stress values. When the initial healing period is 6 months instead of 1 month, large cracks reached higher Sealing Index values for the same exposure condition. However, in both cases a clear trend is not remarkable, since the equivalent nominal tensile stress of each cycle ($\sigma_{eq,cycle}$) is a parameter depending also to fiber orientation (main alignment of fibers with respect to the fracture plane), leading each specimen to have a very different post-cracking response as compared to the other one. This makes very difficult to evaluate the influence of the Sealing Index on SFRC performances since the values of equivalent nominal tensile stress are affected by fiber orientation.

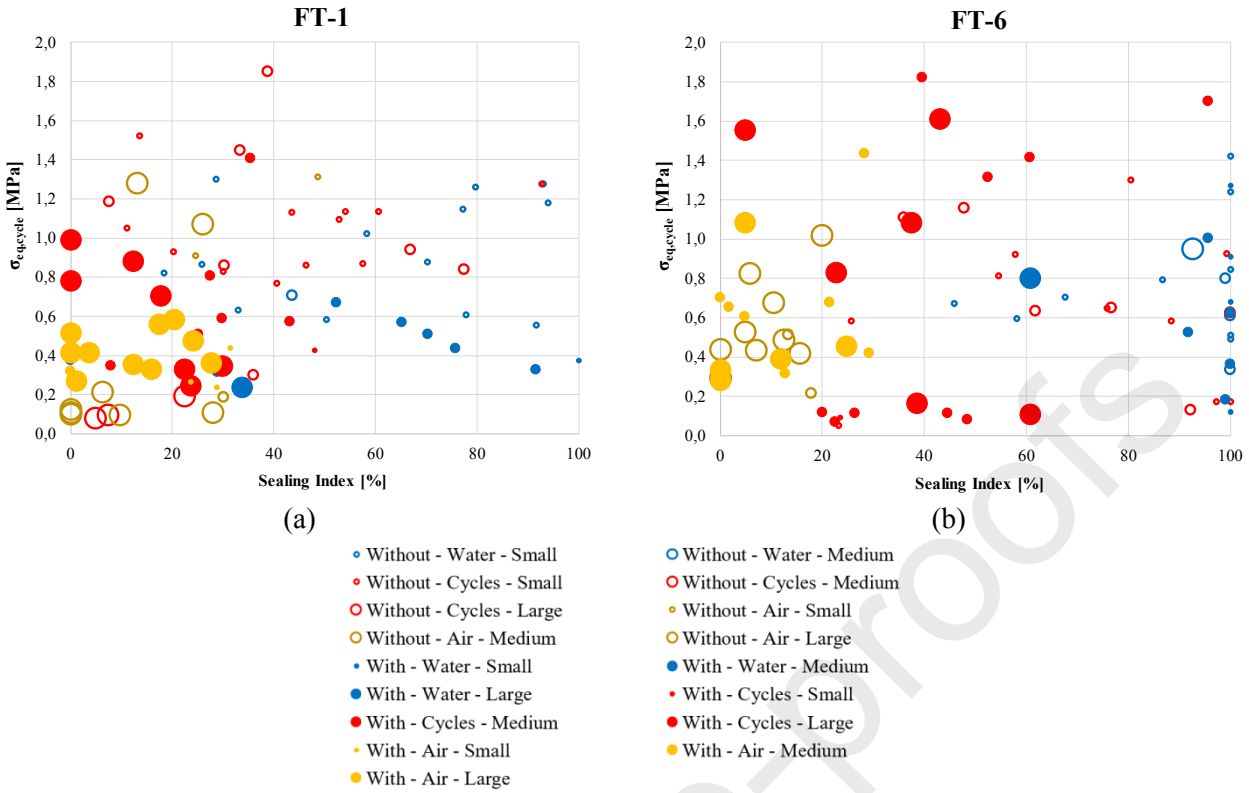

Figure 7. Equivalent tensile stress for each cycle ($\sigma_{eq,cycle}$) versus Sealing Index for: FT-1 (a) and FT-6 (b)

4.2 Normalized cycle-equivalent tensile stress

In order to make the results more comparable one to each other, the equivalent stress value of each cycle ($\sigma_{eq,cycle}$) was normalized by a parameter representing the overall post-cracking response of the specimen, i.e. total equivalent stress value ($\sigma_{eq,total}$). In this way, the influence of fiber orientation is considered since the relative equivalent tensile stress ($\sigma_{eq,cycle}/\sigma_{eq,total}$) represents the post-cracking capacity of each cycle as respect to the overall one, where both of them are characterized by the same fiber orientation. This makes post-cracking performances more comparable. In particular, from the values $W_{F,cycle}$ and $W_{F,total}$, $\sigma_{eq,cycle}$ and $\sigma_{eq,total}$ were obtained (Eq 2). Then, the relative equivalent tensile stress for each cycle was evaluate as:

$$\text{Relative equivalent tensile stress} = \frac{equivalent\ tensile\ stress\ for\ one\ cycle}{total\ equivalent\ tensile\ stress} = \frac{\sigma_{eq,cycle}}{\sigma_{eq,total}} \quad \text{(Eq.4)}$$

In Figure 8 the relative equivalent tensile stress versus Sealing Index was plotted for each exposure condition (water immersion, wet/dry cycles and air exposure) and for both sample groups (FT-1 and FT-6) to do an in-depth analysis. For all these cases, the results represented are distinguished in function of the following parameters:

- With or without crystalline admixture;
- Exposure condition for healing: open air exposure, water immersion or wet/dry cycles;
- Crack width size: small cracks (<0.15mm), medium cracks (0.15-0.30mm) and large cracks (>0.30mm).

The duration of the first healing period (1 or 6 months) has an important influence on the results regarding the Sealing Index, especially for those specimens immersed in water. For FT-6 specimens (Figure 8b) Sealing Index values were from 43% to 100% whereas FT-1 specimens (Figure 8a) showed a wider range of Sealing Index values (from 0 to 100%). The values of relative equivalent tensile stress ranged from 0.4 to 1.1 in both cases (FT-1 and FT-6).

The case of specimens subjected to wet/dry cycles was not so polarized compared to the other conditions (air exposure and water immersion). For wet/dry cycles the values regarding to FT-1 specimens mostly ranged from 0 to 90% (Figure 8c) and FT-6 (Figure 8d) specimens ranged mostly from 5 to 100%. In this case the presence of crystalline admixtures had a positive influence, mainly for larger crack openings. Large cracks from FT-1 reached 0.7 of relative equivalent tensile strength whereas FT-6 reached values even slightly higher than 1.

Specimens exposed to air (FT-1, Figure 8e and FT-6, Figure 8f), generally did not reach Sealing Index values higher than 30%. The presence of crystalline admixture in specimens subjected to open air did not affected the Sealing Index but it affected positively the relative equivalent tensile strength, since specimens with crystalline admixtures reached higher values of relative equivalent tensile strength compared to those without crystalline admixtures for the same level of Sealing Index.

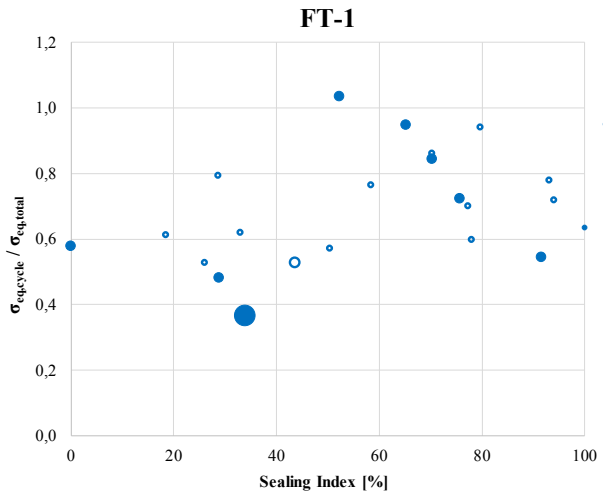

(a)

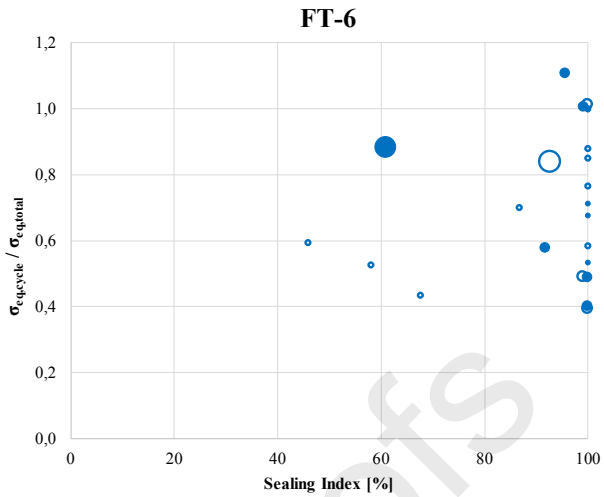

(b)

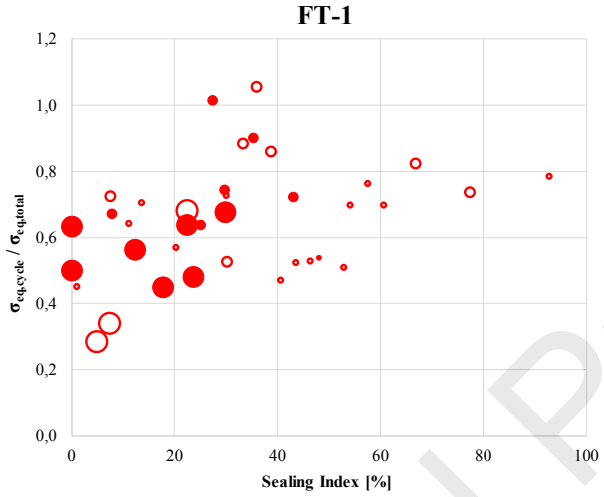

(c)

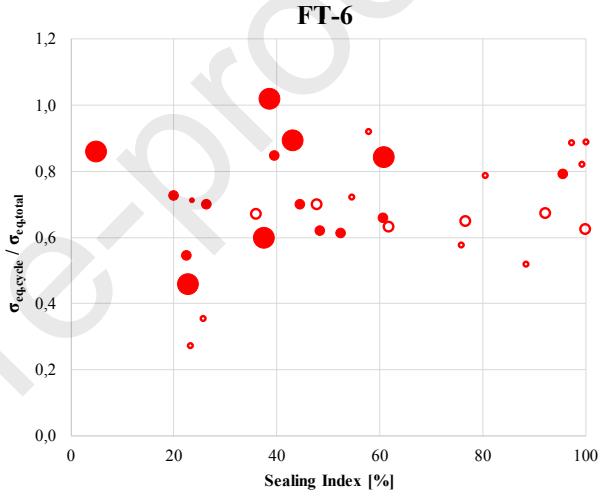

(d)

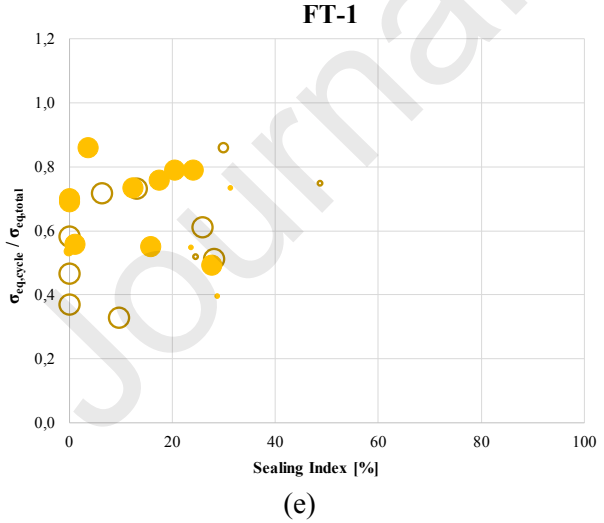

(e)

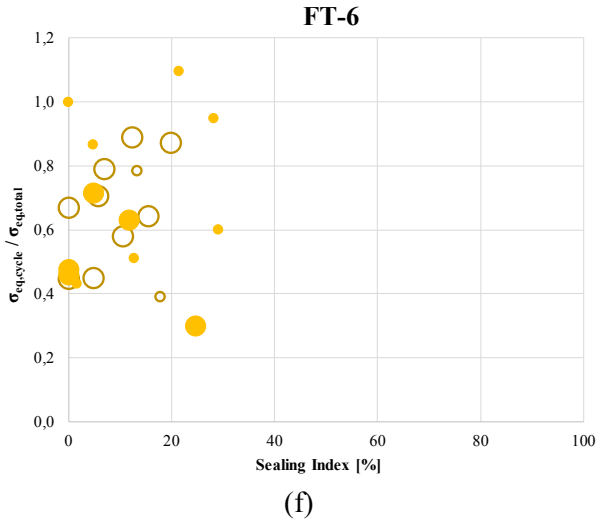

(f)

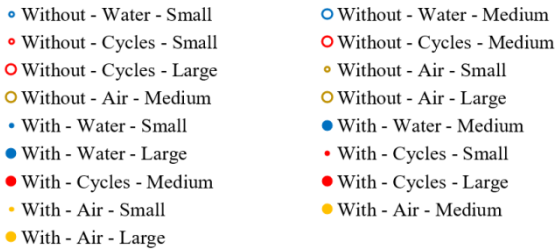

Figure 8. Relative equivalent tensile stress $\sigma_{eq,cycle}/\sigma_{eq,total}$ versus Sealing Index for each exposure condition: water [FT-1 (a), FT-6 (b)], cycles [FT-1 (c), FT-6 (d)] and air [FT-1 (e), FT-6 (f)].

Regarding the crystalline admixture, the effects of its presence were more relevant for less favorable healing conditions, such as wet/dry cycles (Figures 8c and 8d) and open-air exposure (Figures 8e and 8f). In those conditions, it was generally observed that, for the same value of Sealing Index and same crack width size, the values of relative toughness indices are higher when crystalline admixtures are present.

$\sigma_{eq,cycle}/\sigma_{eq,total}$ versus Sealing Index have been plotted in Figure 9, in this case differentiating by crack width size (small, medium or large) instead of exposure condition. For small cracks the Sealing Index was 0-100% and 20-100% for FT-1 (Figure 9a) and FT-6 (Figure 9b) respectively. For medium cracks 0-90% (FT-1) and 0-100% (FT-6). For large cracks 0-35% (FT-1) and 0-90% (FT-6). It can be generally observed that for medium (Figure 9c and 9d) and large cracks (Figure 9e and 9f) and in the case of all three exposure conditions, specimens with crystalline admixtures reached higher values of ($\sigma_{eq,cycle}/\sigma_{eq,total}$) for the same value of Sealing Index.

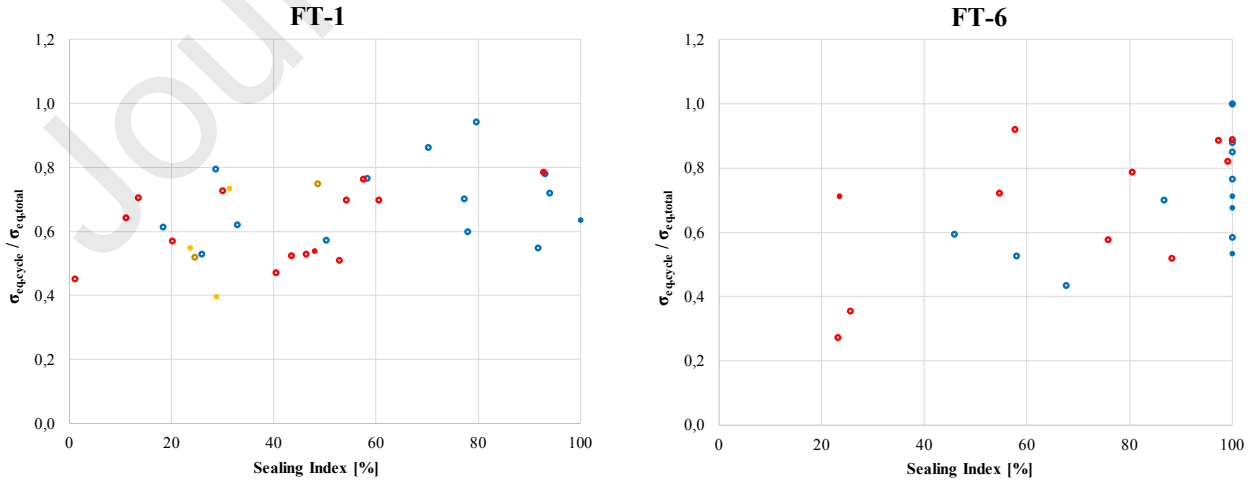

(a) (b)

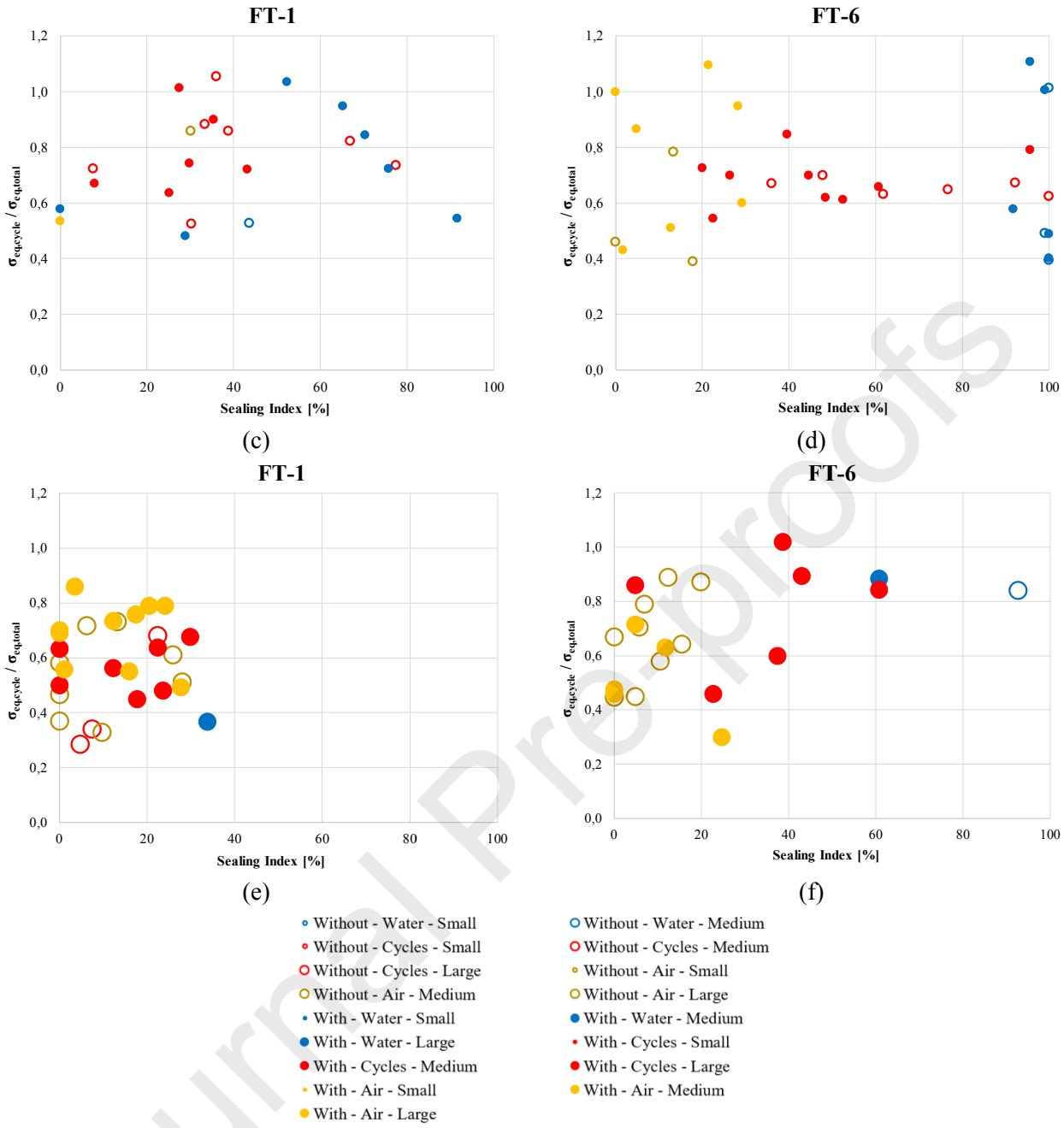

Figure 9. Relative equivalent tensile stress $\sigma_{eq,cycle}/\sigma_{eq,total}$ versus Sealing Index for each crack opening size: small [FT-1 (a), FT-6 (b)], medium [FT-1 (c), FT-6 (d)] and large [FT-1 (e), FT-6 (f)].

According to the results observed in Figure 9, it can be observed that, for the same level of Sealing Index, higher $\sigma_{eq,cycle}/\sigma_{eq,total}$ values were reached for medium size cracks, compared to small ones. A possible explanation of this phenomenon could be that, when cracks are small (<0.15mm) water induces an earlier healing at the very surface of the crack, then preventing any further ingress and continued healing, as compared to medium cracks (0.15-0.30mm). Accordingly, for water immersion exposure condition the cracks only sealed, because they were

close or partially close only on the surface of the specimen. On the other hand, in medium cracks (0.15-0.30mm) water enter across the crack easily than for the case of small cracks, therefore cracks are not only sealed on surface but also healed inside. As a matter of fact, medium cracks reached $\sigma_{eq,cycle}/\sigma_{eq,total}$ values higher than 1, whereas these values did not exceed the unit for the case of small cracks.

4.3 Comprehensive data analysis

In order to find a general trend, Figure 10 plots the relative equivalent tensile stress ($\sigma_{eq,cycle}/\sigma_{eq,total}$) versus Sealing Index for both sample groups (FT-1 in Figure 10a and FT-6 in Figure 10b) where a comprehensive picture of the phenomenon and of the obtained trends could be got. It can be observed that in both healing paths (FT-1 and FT-6), an increment of Sealing Index results in a slight increase (+10-15%) of relative equivalent tensile stress for the studied values of crack widths and environment condition (water immersion, wet/dry cycles, air exposure), even if a strong correlation between the two parameters is not possible. In addition, this slight increment is more remarkable up to a Sealing Index of about 60-70%, after which no further significant increments of relative equivalent tensile stress are appreciable. The reason of this positive effect is probably due to the improved bond between fiber and matrix (improved control of fiber pull-out through the deposition of the healing products along the fiber-matrix interface) as a consequence of self-healing treatments. This is coherent with related findings in the literature [18], [19]. Therefore, the Sealing Index is a factor that slightly influences in a positive manner the post-cracking response of SFRC. Concerning the implications to the behavior of SFRC elements, the present results underline that the effect of self-healing on SFRC performances is in any case secondary; leading the self-healing influence more related to crack width control and increased element durability rather then increase of post-cracking load bearing capacity, though its retention along repeated cracking and healing cycles is also of interest in a design-wise perspective and in the framework of a structural performance interpretation of the durability concept.

In addition, in Figure 10a it can be clearly observed that the highest values of Sealing Index corresponded to the smallest crack widths. Moreover, the highest Sealing Indexes were observed for the specimens immersed in water. The lowest Sealing Indexes corresponded to the larger crack widths; moreover, in those cases the relative

equivalent tensile stress values were slightly higher for specimens with crystalline admixtures. In Figure 10b, some differences were observed comparing with Figure 10a. When specimens were subjected to an initial healing period of 6 months (FT-6), in the case of larger cracks they attained different Sealing Index values: the lowest Sealing Index values (up to 22%) for specimens exposed to air, Sealing Index ranging between 5 and 60% were recorded for specimens subjected to wet/dry cycles and between 60 and 93% for specimens immersed in water. When specimens were subjected to an initial healing period of 1 month instead of 6 months, larger cracks reached a maximum Sealing Index of 35% (for all three exposure conditions). Moreover, for specimens FT-6 (Figure 10b) most small cracks (especially those in specimens permanently immersed in water) healed completely, i.e. reached a 100% Sealing Index and kept it along the repeated cracking-healing cycles. On the other hand, for specimens FT-1 (Figure 10a) only a couple of specimens reached the maximum sealing.

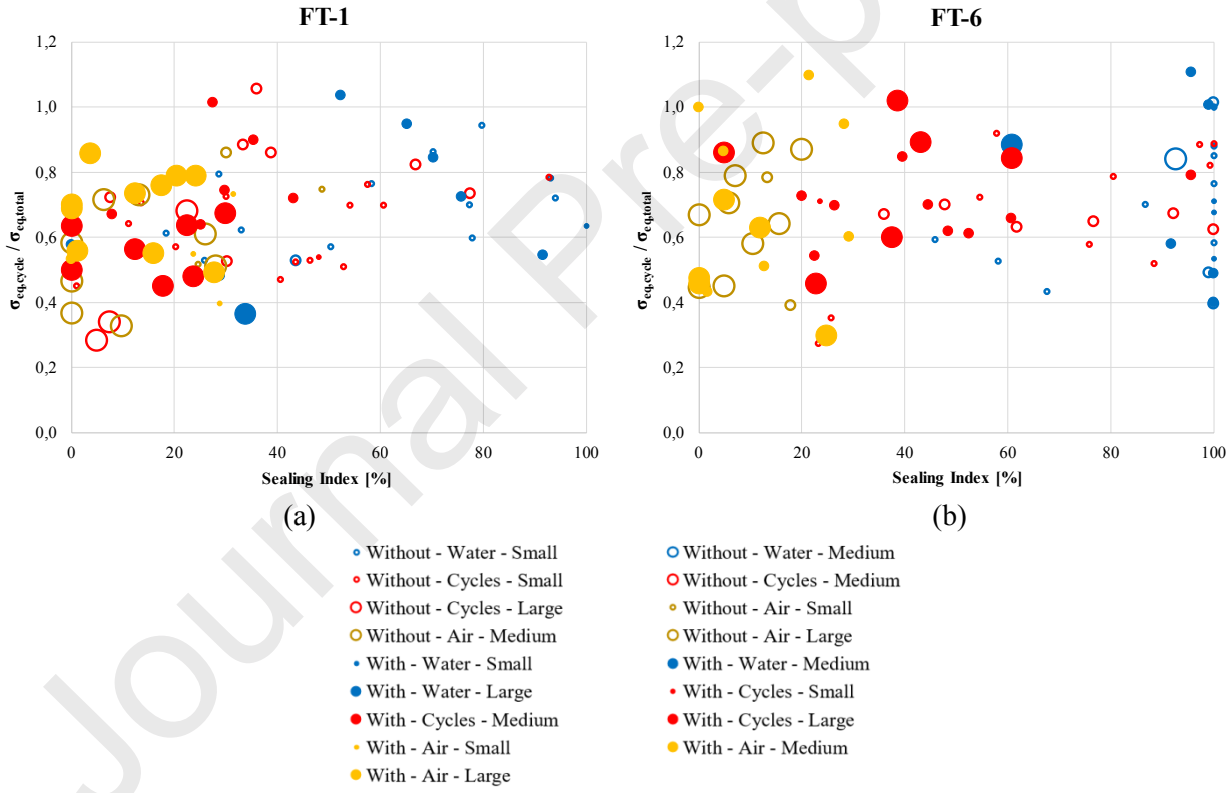

Figure 10. Relative equivalent tensile stress $\sigma_{eq,cycle}/\sigma_{eq,total}$ versus Sealing Index for both sample groups: FT-1 (a) and FT-6 (b)

5. SUMMARY AND CONCLUSIONS

The main objective of this paper has been the assessment of the effects of crack sealing in SFRC with crystalline admixtures under repeated cracking-healing cycles on the fracture toughness parameters. The crack closure after the several cracking-healing periods was quantified by the Sealing Index [%] and this value was related to the mechanical recovery determined from the absorbed energy per unit fracture surface (W_F).

The methodology proposed has yielded consistent results, in line with expectable trends, and was able to capture differences related to the different investigated experimental variables and is hence likely to be applicable for a cross-wise comparison of crack-sealing vs. mechanical and/or durability healing performance data in a wider context. This also with the aim of consistently formulating a scenario-based "healable crack width concept" which could be the pivot point of a durability based design approach incorporating the effects of crack-sealing and material healing.

With reference to the analysis of the specific results obtained in this study, the following conclusions can be drawn:

1. The exposure condition and the initial crack width are key factors for crack sealing. The water immersion condition resulted the most efficient for sealing, reaching very high Sealing Index [%] values up to 100%. The smaller the initial crack opening, the greater Sealing Index. For other conditions, such as open-air exposure and wet/dry cycles, Sealing Index values were lower, especially for air exposure and larger cracks that generally did not reach Sealing Index values higher than 30%.
2. The Sealing Index is a factor positively influencing the SFRC performances. An increase of Sealing Index results in a slight increment of FRC performances (absorbed energy per unit fracture surface) for a given range of crack widths and environment conditions (water immersion, wet/dry cycles, air exposure). This influence seems not to be influenced by treatment procedure (FT-1 or FT-6), as well as a distinct correlation between parameters was not obtainable but is surely something highly needed in a meta-analysis perspective of the large amount of results available in the literature.
3. The influence of self-healing in a real structural element is supposed to be more related to crack width control and improved durability, since the post-cracking performances of SFRC seems to be more

influenced by matrix, fiber type/amount and fiber orientation as compared to Sealing Index. Though the retention of the post-cracking load-bearing capacity along repeated cracking and healing cycles is also of interest in a design-wise perspective and in the framework of a structural performance interpretation of the durability concept.

REFERENCES

[1] C. Meyer, The greening of the concrete industry, Cement and Concrete Composites, 31 (8) (2009) 601-605.

[2] P. Van den Heede, B. Van Belleghem, M. De Keersmaecker, A. Adriaens, N. De Belie, Sustainability effects of including concrete cracking and healing in service life prediction for marine environments, Sustainable Construction Materials and Technologies (2016).

[3] V.C. Li, E. Herbert, Robust self-healing concrete for sustainable infrastructure, Journal of Advanced Concrete Technology, 10 (6) (2012) 207-218.

[4] F. Ortiz-Navas, J. Navarro-Gregori, G. Leiva-Herdocia, P. Serna, E. Cuenca, An experimental study on the shear behaviour of reinforced concrete beams with macro-synthetic fibres, Construction and Building Materials 169 (2018) 888-899.

[5] Ferrara, L., Van Mullem, T., Alonso, M.C., Antonaci, P., Borg, R.P., Cuenca, E., Jefferson, A., Ng, P.L., Peled, A., Roig, M., Sanchez, M., Schroefl, C., Serna, P., Snoeck D., Tulliani, J.M. and De Belie, N.: "Experimental characterization of the self-healing capacity of cement based materials and its effects on the material performance: a state of the art report by COST Action SARCOS WG2", Construction and Building Materials, 167 (2018) 115-142.

[6] De Belie, N., Gruyaert, E., Al-Tabbaa, A., Antonaci, P., Baera, C., Bajare, D., Darquennes, A., Davies, R., Ferrara, L., Jefferson, T., Litina, C., Miljevic, B., Otlewska, A., Ranogajec, J., Roig-Flores, M., Pain, K., Lukowski, P., Serna, P. Tulliani, J.M., Vucetic, S., Wang, J., Jonkers, H.M.: "A review of self-healing concrete for damage management of structures", Advanced Materials and Interfaces, 5(17) (2018) 1-28.

[7] Self-Healing Phenomena in Cement-Based Materials, State-of-the-Art Report of RILEM Technical Committee 221-SHC: Self-Healing Phenomena in Cement-Based Materials, Springer, ISBN: 978-94-007-6623-5, 2013.

[8] Nishiwaki, T., Kwon, S., Homma, D., Yamada, M., and Mihashi, H. (2014). "Self-healing capability of fiber-reinforced cementitious composites for recovery of watertightness and mechanical properties." Materials, 7, 2141-2154

[9] Sahmaran, M., Yildirim, G., Noori, R., Ozbay, E., and Lachemi, M. (2015). "Repeatability and pervasiveness of Self-Healing in Engineered Cementitious Composites." ACI Materials Journal, 112(4) 513-522.

[10] Yang, Y., Lepech, M., Yang, E., and Li, V. (2009). "Autogenous healing of engineered cementitious composties under wet-dry cycles." Cement and Concrete Research, 39, 382-390.

[11] Wu, M., Johannesson, B., and Geiker, M. (2012). "A review: Self-healing in cementitious materials and engineered cementitious composite as a self-healing material." Construction and Building Materials, 28, 571-583

[12] Yildirim, G., Keskin, O., Keskin, S., Sahmaran, M., and Lachemi, M. (2015). "A review of intrinsic self-healing capability of engineered cementitious composites: Recovery of transport and mechanical properties." Construction and Building Materials, 101, 0- 21.

[13] Cuenca, E.A. and Ferrara, L.: "Self-healing capability of Fiber Reinforced Concretes. State of the art and perspectives", Journal of the Korean Society of Civil Engineers, 21(7) (2017) 2777-2789.

[14] E. Cuenca, A. Tejedor, L. Ferrara, A methodology to assess crack-sealing effectiveness of crystalline admixtures under repeated cracking-healing cycles in Fiber Reinforced Concrete, Construction and Building Materials 179 (2018) 619-632.

[15] M. Di Prisco, L. Ferrara, M. Lamperti, Double edge wedge splitting (DEWS): an indirect tension test to identify post-cracking behaviour of fibre reinforced cementitious composites, Materials and Structures 46 (2013) 1893-1918.

[16] A. Hillerborg, The theoretical basis of a method to determine the fracture energy Gf of concrete, Materials and Structures 18(106) (1985) 291-296.

[17] L. Ferrara, V. Krelani, M. Carsana, A fracture testing based approach to assess crack healing of concrete with and without crystalline admixtures, Construction and Building Materials 68 (2014) 535–551.

[18] D. Kim, S. Kang, T. Ahn, Mechanical characterization of high-performance steel-fiber reinforced cement composites with self-healing effect, Materials 7 (1) (2014) 508–526.

[19] M. Li, V. Li, Cracking and healing of engineered cementitious composites under chloride environment, ACI Mater. J. 108 (3) (2011) 333–340.

Highlights

Fracture toughness parameters to assess crack healing capacity of fiber reinforced concrete under repeated cracking-healing cycles

By Estefania Cuenca and Liberato Ferrara

Department of Civil and Environmental Engineering, Politecnico di Milano, Italy

1. Effects of self-healing in fibre reinforced concrete are cross analysed by means of crack closure and capacity of retaining, along cracking and healing cycles, the post-cracking residual load bearing capacity; this is, to authors' knowledge, a one of a kind approach in the literature on self-healing of cement based materials.
2. Novel testing methodology, called Double Edge Wedge Splitting test, is employed for mechanical characterization of tensile behaviour and self-healing capacity of fibre reinforced concrete
3. Full data base is provided in form of tables in the paper